Two-dimensional chaotic thermostat and behavior of a thermalized charge in a weak magnetic field

G. J. Morales
Department of Physics and Astronomy, University of California, Los Angeles, California 90025, USA

(Received 15 April 2019; published 20 June 2019)

A two-dimensional version of a chaotic thermostat is investigated. Its structure follows the concept previously introduced by the author [G. J. Morales, Phys. Rev. E **97**, 032203 (2018)] to generate a one-dimensional chaotic thermostat, namely, the usual friction force of a deterministic thermostat is supplemented with a self-consistent fluctuating force that depends on the drag coefficient associated with coupling to the heat bath. Azimuthal symmetry requires the thermostat to have two internal degrees of freedom, thus the Martyna-Klein-Tuckerman [G. J. Martyna *et al.*, J. Chem. Phys. **97**, 2635 (1992)] model is chosen for the heat bath. The unmagnetized system exhibits two-dimensional diffusive behavior, achieves symmetric Maxwellian velocity distributions in the absence of an external potential, and satisfies the Einstein relation when an external force is applied. The velocity fluctuations display the characteristic exponential frequency spectrum associated with chaotic systems. The model is used to explore the diffusive motion of a thermalized charge in a weak magnetic field and the associated Hall and Pedersen mobilities. Over a range of magnetic field strengths the charge exhibits absolute negative mobility.

DOI: 10.1103/PhysRevE.99.062218

I. INTRODUCTION

A recent publication by the author [1] demonstrated that the inclusion of self-consistent, chaotic fluctuations in a deterministic thermostat [2–5] can better approximate the zero-order behavior of a thermalized particle in one dimension. By zero-order it is meant that in the absence of an external potential or particle-particle interactions, an individual particle self-heats from rest, moves in positive and negative directions executing diffusive behavior, and displays a Maxwellian velocity distribution. In the absence of fluctuations or interactions, the pure deterministic thermostats do not allow for velocity reversals, generate integrable particle orbits, and result in non-Maxwellian velocity distributions. The procedure for achieving the more realistic thermal behavior consists of introducing an additional fluctuating force that is linked to the self-consistent drag coefficient; for deterministic thermostats the drag coefficient varies in time and can be positive or negative. The methodology results in fluctuations that are the chaotic analog of the stochastic fluctuations assumed in the Langevin model. For one dimension the chaotic concept can be implemented for two prominent versions of deterministic thermostats: the Nosé-Hoover [6] and the Martyna-Klein-Tuckerman (MKT) [7] models.

After achieving success with the one-dimensional (1D) case it is natural to inquire if the concept of a chaotic thermostat can be extended to two dimensions. The motivation is that in two dimensions a larger class of phenomena of experimental relevance is possible [8–13], most notably the various effects associated with magnetic forces [14–17]. The present study reports a viable extension of the concept of a chaotic thermostat to two dimensions. Because of the constraint imposed by the requirement of azimuthal symmetry, in this case the venerable Nosé-Hoover model is not suitable. The reason is that the thermostat does not have the two independent degrees of freedom that allow the construction of a chaotic force in two dimensions. Consequently, the MKT model is used since it has an extra degree of freedom.

In the absence of a magnetic field it is found that the proposed two-dimensional (2D) chaotic thermostat exhibits 2D diffusive behavior, achieves symmetric Maxwellian velocity distributions in the absence of an external potential, and satisfies the Einstein relation when an external force is applied. The velocity fluctuations display the characteristic exponential frequency spectrum [18–21] associated with chaotic systems. The model is used to explore the diffusive motion of a thermalized charge in a weak magnetic field and the associated Hall and Pedersen mobilities. Over a range of magnetic field strengths the charge exhibits absolute negative mobility (ANM) [22–27] while displaying a Maxwellian velocity distribution.

The paper is organized as follows. Section II introduces the mathematical form of the model and its natural scaling. In Sec. III the model properties are illustrated by numerical solutions in the absence of a magnetic field. The behavior of a thermalized charge in a weak magnetic field is explored in Sec. IV. Conclusions are presented in Sec. V.

II. MODEL

In a 2D, Cartesian coordinate system (x, y) the equations of motion for a nonrelativistic particle interacting with a chaotic thermostat, in the absence of external forces and particle-particle interactions, take the form

$$m\frac{dv_x}{dt} = F_x - \gamma(t)mv_x, \tag{1}$$

$$m\frac{dv_y}{dt} = F_y - \gamma(t)mv_y, \tag{2}$$

where m is the particle mass, v_j and F_j are the jth components of the particle velocity and fluctuating force, respectively, and

γ is the drag (or damping) coefficient provided by the heat bath to thermalize the particle motion. As mentioned in the Introduction, the MKT model is used to govern the evolution of γ because it includes an additional degree of freedom that is necessary to obtain a suitable fluctuating force in two dimensions. The corresponding thermostat variables (γ, η) evolve according to

$$\frac{d\gamma}{dt} = t_0^{-2}\left(\frac{v_x^2 + v_y^2}{\bar{v}^2} - 2\right) - \eta\gamma, \tag{3}$$

$$\frac{d\eta}{dt} = \alpha^{-2}\left(\frac{\gamma^2}{\gamma_0^2} - 1\right), \tag{4}$$

in which the average thermal velocity per degree of freedom is $\bar{v} = \sqrt{T/m}$ for a heat bath of temperature T. The parameter t_0 corresponds to the timescale for coupling between the particle and the heat bath; here it is considered to be the key scaling quantity that represents the system. The parameter α is, in principle, a separate timescale for coupling to a second thermostat whose role is to internally regulate the thermalization of the drag coefficient whose average value is γ_0. This study considers the universally scaled case in which a single timescale controls the interaction with the heat bath, i.e., $\gamma_0 t_0 = 1$, $\alpha = t_0$.

Following the successful procedure previously used in generating a 1D chaotic thermostat for the MKT model [1], two phase angles (θ, ϕ) are linked to the individual damping coefficients (γ, η) through the relations

$$\frac{d\theta}{dt} = \gamma(t), \tag{5}$$

$$\frac{d\phi}{dt} = \eta(t). \tag{6}$$

The general features of the stochastic Langevin force provide guidance in searching for a viable chaotic analog, namely, the fluctuating force should have zero mean and have a short autocorrelation, and the product of the (x, y) components should average to zero. In addition, the force should result in azimuthally symmetric responses in two dimensions. After extensive numerical tests with candidate forms it has been found that the following combination meets the desired requirements:

$$F_x = F_0(\cos\theta - \cos\phi), \tag{7}$$

$$F_y = F_0(\sin\theta + \sin\phi), \tag{8}$$

where the constant amplitude F_0 is chosen to provide optimal thermal behavior (i.e., accurate Maxwellian distributions are obtained in the x and y directions).

A figurative analogy useful in attaching a physical picture to the role played by Eqs. (7) and (8) is that of a panicked driver, sliding on an icy parking lot while trying to keep moving at a chosen average speed. The driver executes conscious (i.e., deterministic) attempts at steering the car right and left while simultaneously stabbing the brake and accelerator pedals, which are represented here by the linked positive and negative spikes of γ in Eq. (1). This is a deterministic chaotic process to be contrasted to the popular picture of the Langevin model as resembling a drunkard taking steps in random directions in two dimensions.

The natural scaling of the system is implemented through the following scaled variables and parameters:

$$\tau = \frac{t}{t_0}, \quad u_j = \frac{v_j}{\bar{v}}, \quad \Gamma = \gamma t_0, \quad s = \eta t_0, \quad \lambda = \frac{F_0 t_0}{m\bar{v}}, \tag{9}$$

resulting in

$$\frac{du_x}{d\tau} = \lambda(\cos\theta - \cos\phi) - \Gamma u_x, \tag{10}$$

$$\frac{du_y}{d\tau} = \lambda(\sin\theta + \sin\phi) - \Gamma u_y, \tag{11}$$

$$\frac{d\Gamma}{d\tau} = \left(u_x^2 + u_y^2 - 2\right) - s\Gamma, \tag{12}$$

$$\frac{ds}{d\tau} = \Gamma^2 - 1, \tag{13}$$

$$\frac{d\theta}{d\tau} = \Gamma, \tag{14}$$

$$\frac{d\phi}{d\tau} = s. \tag{15}$$

The system of Eqs. (10)–(15) has two possible fixed points that can be identified by direct inspection. For the case $\phi_0 = -\theta_0$, $u_{x0} = u_{y0} = 0$, $\Gamma_0 = \pm 1$, $s_0 = \pm 2$, and arbitrary λ, the heat baths execute damped oscillations with a scaled frequency $f_0 = \sqrt{2}/2\pi = 0.1125$ without involvement of the material particle. For values of $\lambda > 1/\sqrt{2} = 0.7071$, a fixed point at $\Gamma_0 = \pm 1$, $s_0 = 0$, corresponding to cold beams with $u_{x0}^2 + u_{y0}^2 = 2$, is found for phases that satisfy the condition $\cos(\theta + \phi) = 1 - \lambda^{-2}$.

Inclusion of a uniform magnetic field B perpendicular to the (x, y) plane, for a particle of charge q and mass m, suggests the use of a complex velocity variable $V = u_x + iu_y$, that transforms Eqs. (10)–(12) into the compact form

$$\frac{dV}{d\tau} = \lambda(e^{i\theta} - e^{-i\phi}) - (\Gamma - iw)V, \tag{16}$$

$$\frac{d\Gamma}{d\tau} = (|V|^2 - 2) - s\Gamma, \tag{17}$$

where the scaled cyclotron frequency is $w = qBt_0/mc$.

In numerical studies to be presented in the following sections the value $\lambda = 0.35$ is used. This choice is found to provide the best thermal behavior for both the unmagnetized and magnetized cases. For much smaller and larger values of λ, the system is not chaotic, and accordingly the velocity distribution functions are far from being Maxwellian. It is to be noted that in the previous 1D study the equivalent value of λ was 0.5. Such a value also yields satisfactory thermal results (i.e., near-Maxwellian distributions) but that are not as good (the fitting Maxwellians have deviations in the thermal velocity of 5%) as those shown in the following sections.

III. UNMAGNETIZED MODEL PROPERTIES

The numerical results presented in this and the following sections are obtained by solving Eqs. (10)–(15) with a fourth-order Runge-Kutta method using a scaled time step $d\tau = 10^{-3}$, as is typical of similar studies. Characteristically, the

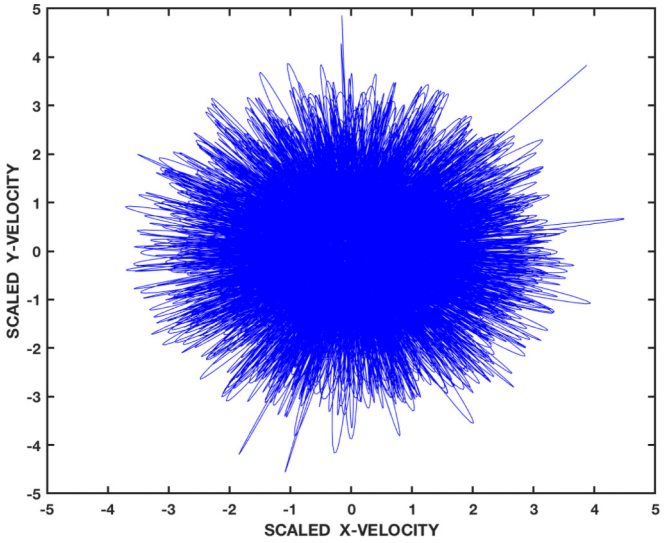

FIG. 1. Instantaneous values of scaled y and x velocities over a time interval $\tau = 10\,000$ for one realization of the ensemble illustrate the high degree of symmetry resulting from the chaotic fluctuations. Rare and infrequent phase conditions cause the temporary attainment of energies well beyond the thermal energy.

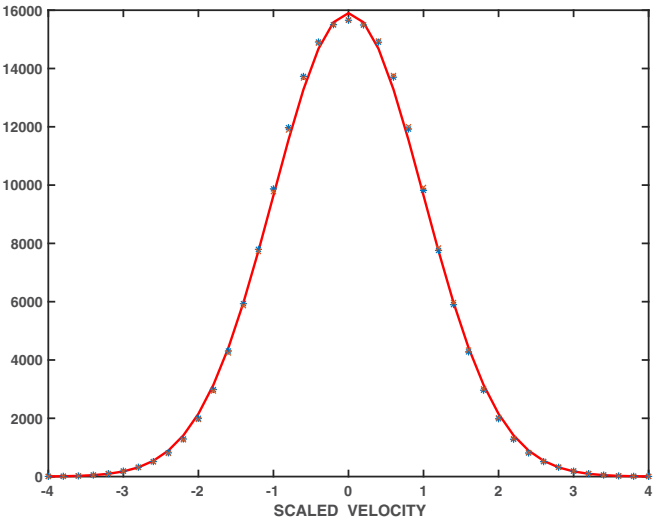

FIG. 2. Ensemble-averaged velocity distribution functions in the y and x directions are represented by the different discrete symbols arranged in 41 bins. They are obtained from individual realizations of the type shown in Fig. 1. The red curve is a Maxwellian function with scaled, square average velocity equal to 1. Comparison demonstrates that the velocity distribution functions generated by the chaotic fluctuations are spatially symmetric and closely approximate the thermal equilibrium value.

calculations are stored every 50 steps for further analysis, for a total time record of $\tau = 10\,000$. When performing averages, 20 initial values of θ and of ϕ, distributed uniformly in $(0, 2\pi)$, are sampled, for a choice of 11 initial velocities distributed uniformly along a 45° line in the (x, y) plane including zero velocity; this corresponds to an ensemble of 4400 realizations. All the cases are started from $\Gamma = 0$, $s = 0$.

The high degree of azimuthal symmetry resulting from the 2D chaotic fluctuations, described by Eqs. (7) and (8), is illustrated in Fig. 1. Shown are the instantaneous values of the scaled, y, and x velocities (providing one dot on the plane of the figure) over a time interval $\tau = 10\,000$ for one realization in the ensemble, i.e., it is not an average. It is also seen in Fig. 1 that some infrequent conditions result in the momentary attainment of energies well beyond the average thermal energy. From individual time series associated with the typical behavior shown in Fig. 1, the average velocity distribution functions in the y and x directions are obtained. In Fig. 2 the continuous red curve corresponds to a Maxwellian function of zero mean, and with a squared, scaled velocity equal to 1, i.e., $\langle u_j^2 \rangle = 1$, where $j = x$ or y. The discrete symbols are the individual values of the calculated, average distribution functions in both the y and x directions, each arranged in 41 bins. Two different symbols are used for y and x in Fig. 2, but the results overlap. It is seen that the velocity distributions are spatially symmetric and closely follow the thermal equilibrium value. The numerical values obtained from the direct ensemble average are $\langle u_y^2 \rangle = \langle u_x^2 \rangle = 0.98$, and $\langle u_y \rangle = 4.81 \times 10^{-4}$, $\langle u_x \rangle = 2.49 \times 10^{-4}$, consistent with the finite size of the ensemble and numerical accuracy.

The autocorrelation functions of the y (red curve) and x (black curve) scaled velocities (indicated by the symbol "u"), and of the scaled damping coefficient Γ (blue curve), are displayed in Fig. 3 for a single realization, i.e., not averaged. It is seen that the results for the two velocity directions are essentially identical, attesting again to the azimuthal symmetry of the system. The 2D chaotic fluctuations cause the velocity to become decorrelated on a timescale of $\tau \approx 10$, which is similar to the result found previously for one dimension. But the damping coefficient displays a much longer decorrelation time, which results in coherent features in the velocity fluctuation spectra that are discussed later.

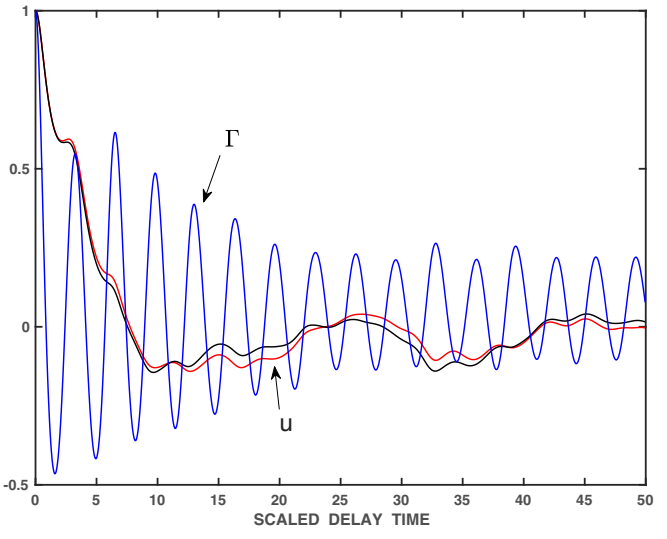

FIG. 3. Autocorrelation functions of the y (red curve) and x (black curve) scaled velocities indicated by the symbol "u," and of the scaled damping coefficient Γ (blue curve), for a single realization, i.e., not averaged.

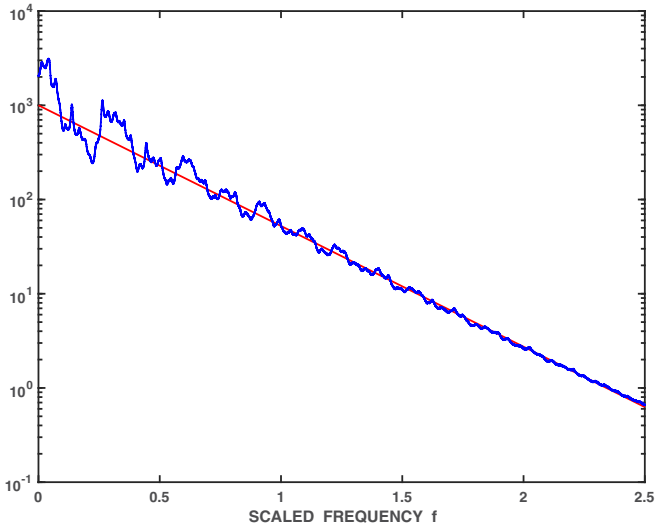

FIG. 4. Log-linear display of the ensemble-averaged amplitude of the frequency spectrum of the scaled, x velocity, i.e., $\langle|\tilde{u}_x(f)|\rangle$, for the unmagnetized case, $(w = 0)$, is shown as the continuous blue curve. Frequency f is scaled to t_0^{-1}. Red straight line is an exponential fit of the form $\exp(-2\pi\tau_L f)$ with $\tau_L = 0.47$; it indicates that the velocity fluctuations are chaotic.

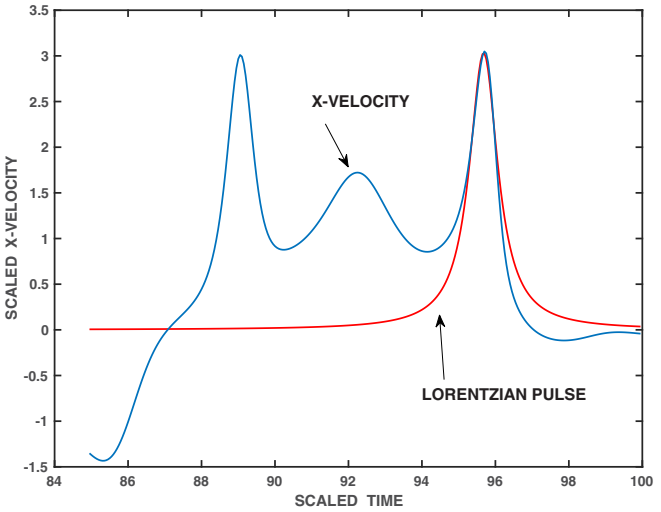

FIG. 5. Scaled x velocity (blue curve), for one realization, is displayed over a small time segment that is arbitrarily chosen. The red curve is a Lorentzian function given by Eq. (18) in which the width is identical to the independently determined width from the slope of the red line that provides an exponential fit to the ensemble-averaged spectrum in Fig. 4. The presence of the Lorentzian pulses shows that the underlying dynamics is chaotic. Similar results, not shown, are found for the y velocity.

The ensemble-averaged amplitude of the frequency spectrum of the x component of the scaled velocity, i.e., $\langle|\tilde{u}_x(f)|\rangle$ is displayed in log-linear format in Fig. 4, with the scaled frequency f in units of t_0^{-1}. The equivalent quantity for the y velocity is identical; thus for brevity it is not shown. The reason for the log-linear display is to identify the characteristic signature of a chaotic system, namely, an exponential frequency dependence [18–21], which in such a display appears as a straight line. The red line in Fig. 4 is proportional to the function $\exp(-2\pi\tau_L f)$, for the fitted value of $\tau_L = 0.47$; it provides an excellent fit to the baseline of the frequency spectrum. But at the lower frequencies this baseline is punctuated by a complex pattern of coherent oscillations that are discussed later in Sec. IV. The significance of the exponential spectrum is that it arises from unique Lorentzian pulses associated with chaotic dynamics [20,21] and having the temporal form

$$L(\tau) = \frac{A\tau_L^2}{(\tau - \tau_j)^2 + \tau_L^2}, \tag{18}$$

in which A represents the peak amplitude of a pulse appearing at time τ_j and having a width τ_L. The presence of such Lorentzian pulses in the particle dynamics is confirmed in Fig. 5, where a small segment, $84 \leqslant \tau \leqslant 100$, of the time series of the scaled x velocity (blue curve) is displayed for one realization of the ensemble. The localized red curve in Fig. 5 is the expression given by Eq. (18) for a peak centered at $\tau_j = 95.68$, with amplitude $A = 0.67$ and, significantly, with a width identical to the value obtained independently from the exponential fit to the ensemble-averaged spectrum in Fig. 4, i.e., $\tau_L = 0.47$. Similar fittings can be made at other arbitrarily chosen segments of the time series and for the scaled y velocity. It should be noted that the Lorentzian pulses, of positive and negative polarity, are embedded in a background of coherent oscillations corresponding to the spectral peaks seen in Fig. 4.

The typical spatial pattern of the "walk" associated with the 2D chaotic fluctuations is exemplified by the blue curve, labeled $w = 0$, in Fig. 6. Each point on the curve corresponds to the instantaneous (x, y) position for one realization in the absence of magnetic field. For comparison the equivalent walk in the presence of a finite magnetic field, $w = 1.5$, is included and represented by the red curve. The time interval

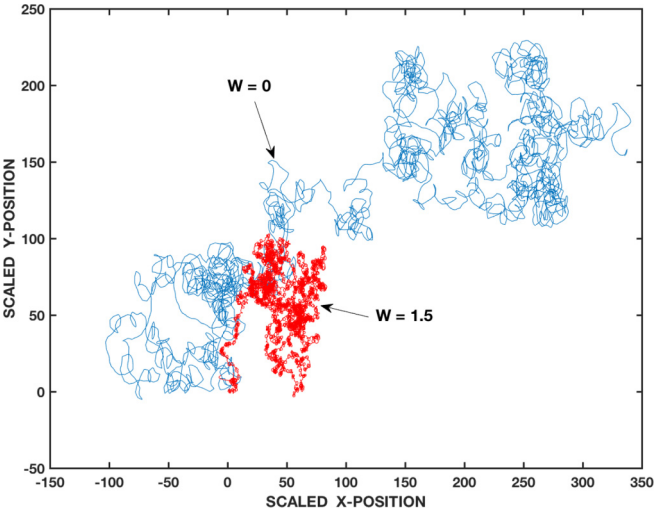

FIG. 6. Illustration of typical 2D walk for an unmagnetized case, $w = 0$ (blue curve), and a magnetized one, $w = 1.5$ (red curve). Each point along a curve is the instantaneous, scaled y and x positions for one realization. The time record for both cases corresponds to $\tau = 10\,000$.

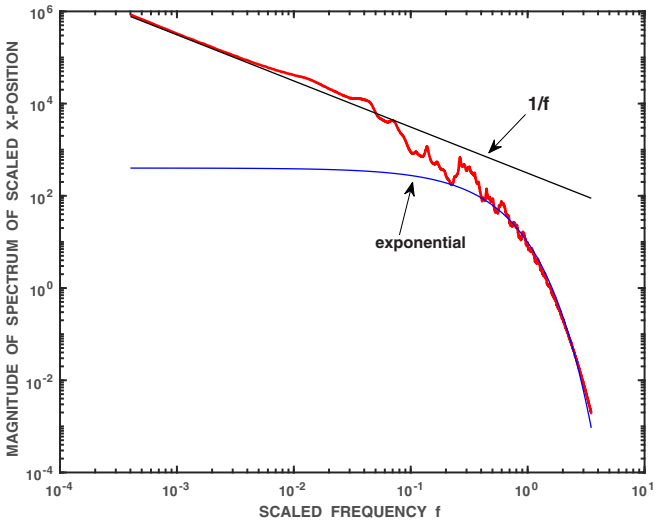

FIG. 7. Frequency dependence of the ensemble-averaged amplitude of the frequency spectrum of the scaled x position, i.e., $\langle|\tilde{x}(f)|\rangle$, is shown as the red curve for an unmagnetized case. Frequency f is scaled to t_0^{-1}. A log-log display format is used to illustrate the different behavior occurring on different timescales. The black curve has a functional form of f^{-1}, and the blue curve is an exponential function of the form $\exp(-2\pi\tau_L f)$ with $\tau_L = 0.57$. Similar results, not shown, are found for the y position.

for both cases is the same, $\tau = 10\,000$. It is evident that the the magnetic force curtails the size of the spatial region sampled by the thermalized particle. Since the unmagnetized (blue) path is larger, it illustrates better that the underlying walk consists of relatively long, but finite, jumps interspersed with periods of relative localization during which smaller steps are taken. The 2D path is not a Lévy flight or walk [28,29], as has been identified in some models of motion in 2D potential barriers [30], nor is it the random walk of the Langevin model. The path followed is intrinsically deterministic, but in practice it is impossible to predict, which is the essence of chaos.

Further insight about the 2D walk is provided by Fig. 7. Shown as a red curve is the ensemble-averaged amplitude of the frequency spectrum of the scaled x position, $\langle|\tilde{x}(f)|\rangle$. But now a log-log display format is used to illustrate the different behavior occurring on different timescales. Two additional curves are included to provide a perspective. The black curve has a functional form of f^{-1}, and the blue curve is an exponential function of the form $\exp(-2\pi\tau_L f)$ with $\tau_L = 0.57$. It is seen that for long timescales, $f < 0.02$, a power-law dependence occurs, which is indicative of stochastic behavior. For short timescales, $f > 0.2$, the spectrum is exponential, which corresponds to chaotic behavior. The stochastic to chaotic transition for timescales corresponding to the frequency range $0.02 < f < 0.2$ exhibits relatively narrow spectral lines associated with coherent behavior. Identical dependencies are found for the y position. For quantitative reference it should be mentioned that the scaled Nyquist frequency for the results shown in Fig. 7 is 10, and the smallest, resolvable scaled frequency is 0.0001.

From an ensemble of paths of the type depicted by the blue curve in Fig. 6, the scaled, spatial diffusion coefficient, D_s, is extracted. The significant finding is that the time evolution of $\langle(\Delta x)^2 + (\Delta y)^2\rangle$ scales linearly with time, i.e., in spite of the deterministic origin of the fluctuations, and the complex nature of the 2D walk, on average, the spatial behavior is diffusive. The result is not shown here as a figure because it was found earlier for one dimension (e.g., Fig. 10 of Ref. [1]), and a more informative figure is presented in Sec. IV for the magnetized case. Implementing the diffusion calculation yields the value $D_s = 1.85$, to be contrasted to a value $D_s = 1.45$, obtained previously (Fig. 10 of Ref. [1]) for the 1D case using an effective value of $\lambda = 0.5$.

For possible future comparisons to other problems, it is useful to express the result obtained for the spatial diffusion coefficient in more general terms. Using a kinetic relaxation model [31] it is found that for a Maxwellian velocity distribution function, the unscaled, diffusion coefficient D is given by the expression $D = \bar{v}^2\langle t_R(v)\rangle$, where the relaxation time, t_R, in general, depends on velocity. From this expression it can be deduced that for the present 2D chaotic model $\langle t_R(v)\rangle \approx 4\tau_L$, where τ_L corresponds to the physical (i.e., un-scaled) temporal width of the Lorentzian pulses in the velocity fluctuations, illustrated in Fig. 5.

To test the Einstein relation between the spatial diffusion coefficient D and the (mechanical) mobility μ, an external force of strength G is applied over a finite time interval $2000 \leqslant \tau \leqslant 9000$, in the same manner previously implemented for the 1D thermostat (e.g., Fig. 11 of Ref. 1). But in addition, in the present 2D study it has been ascertained that the results are independent of the direction in which the applied force points within the (x, y) plane; i.e., the mobility is azimuthally symmetric for the unmagnetized case. It is found that over the practical range of scaled external forces $0.1 \leqslant Gt_0/m\bar{v} \leqslant 0.2$,

$$\frac{D}{\mu T} = \frac{D_s}{\mu_s} = 0.99 \pm 0.07, \tag{19}$$

where $\mu_s = m\mu/t_0$ is the scaled (mechanical) mobility whose average value is 1.9.

IV. MAGNETIZED BEHAVIOR

This section explores the behavior of a charged particle, of charge q and mass m, thermalized through its contact to the 2D chaotic thermostat, but in the presence of a magnetic field whose strength is considered to be "weak." By weak it is meant that the influence of the magnetic field is comparable to that of the heat bath, or in terms of the scaled cyclotron frequency, $w = qBt_0/mc$, in the interval $0.1 < w < 6$. What makes this situation physically interesting, and challenging to describe analytically, is the competition between two opposing dynamical tendencies. The heat bath tries to generate a broad range of velocities that satisfy a Maxwellian distribution, while the magnetic field causes the magnitude of the velocity to remain constant, i.e., it generates a delta-function distribution in energy. The processes through which these two opposing tendencies arrive at a balance exemplify issues of interest in the study of nonequilibrium systems.

There is a long history to the study of Brownian motion in a magnetic field for a classical, charged particle [32–35]. The early studies were based on the Langevin model in which

the velocity drag coefficient γ is time-independent, and two mutually perpendicular, fluctuating forces act on a charge that circulates around a magnetic field. The Langevin fluctuations are assumed to be statistically independent of the velocity and individually represented in the (x, y) directions as white noise that is delta-correlated. Recently, significant attention has been devoted to relaxing these approximations and to exploring the effects of correlated noise [36–39]. The present study, in an extreme sense, belongs to this category.

For reference and perspective in comparing the results of the 2D chaotic model, the magnetized diffusion coefficient D_L obtained from the Langevin model is rescaled; i.e., it becomes D_{Ls}, to agree with the quantities defined in Sec. II,

$$D_L = \frac{\bar{v}^2\gamma}{\gamma^2+\Omega^2}, \quad D_{Ls} = \frac{\Gamma}{\Gamma^2+w^2}. \tag{20}$$

In describing the effects produced by the application of an external electric field vector $\vec{E}$ in the presence of a magnetic field, it is common to use an electrical mobility tensor defined by $\vec{v} = \overleftrightarrow{\mu} \cdot \vec{E}$, which differs from the mechanical mobility discussed in Sec. III by the factor q, the charge. Of relevance to the case where the electric field points along the x direction are the mobility tensor components

$$\mu_{xx} = \frac{q\gamma}{m(\gamma^2+\Omega^2)}, \quad \mu_{xy} = \frac{q\Omega}{m(\gamma^2+\Omega^2)}, \tag{21}$$

which are obtained for a time-independent γ, and where $\Omega = qB/mc$ is the unscaled cyclotron frequency.

Introducing the scaled (electrical) mobility components as $(\mu_{ij})_s = m\mu_{ij}/qt_0$, leads to the definitions

$$(\mu_{xx})_s = \mu_{Ps} = \frac{\Gamma}{\Gamma^2+w^2}, \tag{22}$$

as the scaled, Pedersen mobility, and

$$(\mu_{xy})_s = \mu_{Hs} = \frac{w}{\Gamma^2+w^2}, \tag{23}$$

as the scaled, Hall mobility. A simple relation, used in Sec. IV to infer the effective value of the scaled drag coefficient, is

$$\frac{\mu_{Ps}}{\mu_{Hs}} = \frac{\Gamma}{w}. \tag{24}$$

A property of such a magnetized, Langevin model is that it displays the same value for the Einstein ratio as in the unmagnetized case: $D_{Ls}/\mu_{Ps} = 1$. With this brief background as a reference, the numerical results are discussed next.

The velocity distribution functions, in the x and y directions, generated by the 2D chaotic model for the magnetized case are found to yield a better fit to a Maxwellian function than the already excellent result depicted in Fig. 2 for the unmagnetized case, thus they are not shown. The reason for the slight improvement is that the additive rotation provided by the magnetic field enhances the azimuthal symmetry, e.g., for $w = 2$, it is found that $\langle \bar{u}_y^2 \rangle = \langle \bar{u}_x^2 \rangle = 1.02$, and $\langle u_y \rangle = 1.46 \times 10^{-4}$, $\langle u_x \rangle = -7.35 \times 10^{-5}$.

The frequency spectrum of the velocity fluctuations for the magnetized case exhibits the general characteristics seen in the log-linear display of Fig. 4 for the unmagnetized case ($w = 0$); it consists of a baseline exponential frequency dependence punctuated by coherent, low-frequency peaks. The

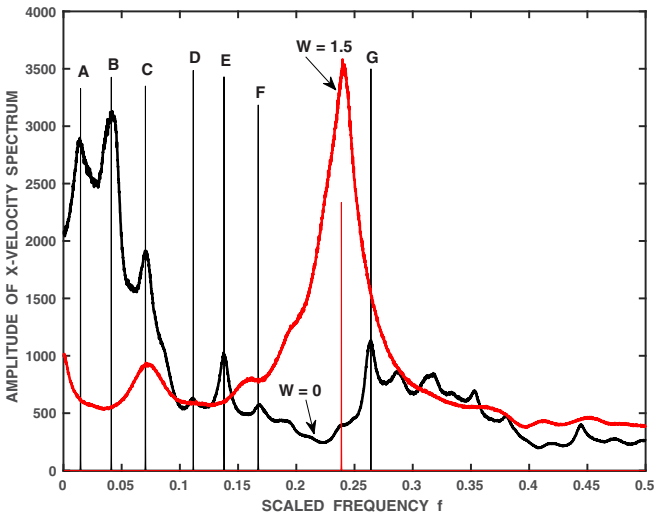

FIG. 8. Comparison of the amplitude of the frequency spectrum of the x velocity for a magnetized case $w = 1.5$ (red curve) to the unmagnetized case $w = 0$ (black curve), using a linear display format in a limited frequency range $f \leqslant 0.5$. Over a larger frequency range the spectrum follows an exponential frequency dependence, as in Fig. 4. The results for the y velocity are identical. The values of the frequencies associated with the A–G peaks are explained in the text. These peaks disappear in the presence of the magnetic field. The unlabeled (red) vertical line corresponds to the scaled cyclotron frequency $f = 1.5/2\pi$. The broadening of the cyclotron resonance seen in the red curve is a manifestation of the chaotic fluctuations.

Lorentzian width of the pulses responsible for the exponential dependence is $\tau_L = 0.44$, which is slightly smaller than for the unmagnetized case, $\tau_L = 0.47$, and thus not worth displaying. But the structure of the coherent peaks is significantly altered in the presence of a magnetic field, as is illustrated in Fig. 8 using a linear display format over the scaled-frequency range $f \leqslant 0.5$. In Fig. 8 the amplitude of the x-velocity frequency spectrum, $\langle |\tilde{u}_x(f)| \rangle$, is shown for $w = 0$ (black curve) and for $w = 1.5$ (red curve); the results for the y-velocity component, not shown, are identical. It is seen that the frequency peaks labeled A, B, D, E, F, and G disappear in the presence of the magnetic field, and the peak labeled C is reduced in amplitude by a factor of 2 and broadened. The numerical value of the frequencies of these unmagnetized peaks is nontrivial but can be cataloged as members of a family having an angular frequency of the the form $2\pi f(n, l) = (' c'/4)(n + l/8)$, with n and l integers, and surprisingly, $' c' = 0.59$ is the peculiar (angular frequency) root identified in Ref. [1], in connection with the Nosé-Hoover thermostat. Apparently, the underlying structure of this other thermostat, upon which the MKT model is based, plays a role in the complex nonlinear frequency mixing. For the record, the following integer assignments generate the frequencies of the lettered peaks in Fig. 8: $A \Rightarrow (0, 5)$, $B \Rightarrow (1, 6)$, $C \Rightarrow (3, 0)$, $D \Rightarrow (4, 6)$, $E \Rightarrow (6, -1)$, $F \Rightarrow (7, 1)$, $G \Rightarrow (11, 2)$. For comparison, there is another unlabeled (red) vertical line shown in Fig. 8; it corresponds to the cyclotron frequency for the magnetized case having $w = 1.5$, i.e., it is $f = w/2\pi$. It should be noted that the individual vertical lines in Fig. 8 are not drawings. They are the Fourier transforms of sinusoidal signals with the frequencies previously described

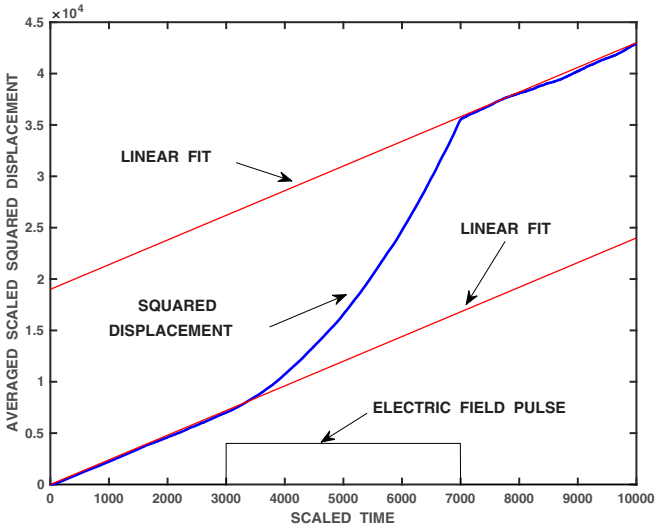

FIG. 9. Demonstration of diffusive behavior in the presence of a magnetic field for $w = 3$. Blue curve labeled "squared displacement" shows the time dependence of the ensemble average of the squared, scaled displacement $\langle x^2 + y^2\rangle(\bar{v}t_0)^{-2}$. Red straight lines are linear fits whose slope is proportional to the diffusion coefficient. The deviation from diffusive behavior, i.e., linear increase with scaled time, is caused by the application of a pulsed electric field, indicated at the bottom. Similar results are obtained over the range $w \leqslant 6$.

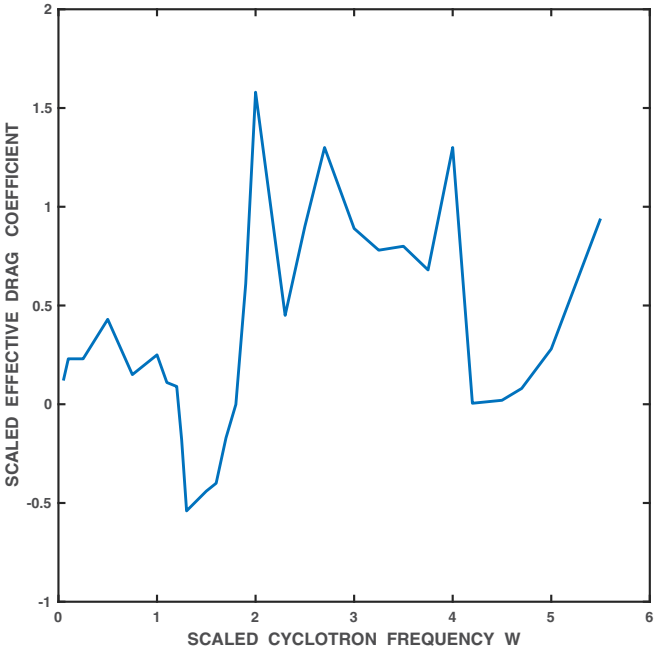

FIG. 10. Magnetic field dependence of effective Langevin drag coefficient obtained from Eq. (24) after calculating μ_{Ps}, and μ_{Hs}, independently, from the 2D chaotic model by applying a scaled electric field $qEt_0/m\bar{v} = 0.1$, as illustrated in Fig. 9. Range of scaled cyclotron frequency is $0.05 \leqslant w \leqslant 5.5$.

and are calculated numerically with the same algorithm used to generate the black and red curves. Thus the broadening seen in the red curve ($w = 1.5$) is not a numerical artifact, but rather it is a manifestation of the broadening of the cyclotron resonance due to the chaotic fluctuations.

The diffusive behavior for the magnetized case is demonstrated in the time dependence shown in Fig. 9 for a scaled magnetic field $w = 3$; similar results hold for all the magnetic field values explored, i.e., $w \leqslant 6$. The (blue) curve labeled "displacement" corresponds to the ensemble average of the scaled displacement $\langle x^2 + y^2\rangle(\bar{v}t_0)^{-2}$. The two oblique, straight (red) lines labeled "linear fit" have the same slope (i.e., they are parallel lines that are vertically displaced); from the value of the slope the scaled diffusion coefficient is extracted. It is seen that the blue curve overlaps the lower straight line over the time interval $0 < \tau < 3000$, and merges with the upper straight line for $\tau > 7000$. During the interval $3000 < \tau < 7000$ the blue curve follows a near-parabolic time dependence (i.e., the charge experiences a drift) because an external electric field pulse is applied during that interval, as indicated by the top-hat function at the bottom of the figure. The scaled value of the applied electric field E is $qEt_0/m\bar{v} = 0.1$, and for this figure it points in the x direction, but the results are independent of field orientation. It is also found, but not shown, that within small fluctuations, the diffusion coefficients in the x and y directions have the same values. It is concluded from the example shown in Fig. 9 that for a weak magnetic field the 2D chaotic model also results in zero-order diffusive behavior. The diffusive behavior is altered by the application of an external electric field but is recovered when the electric field is turned off.

Next, the dependence on the strength of the magnetic field is explored. In contrast to the Langevin model, in the 2D chaotic model the value of the drag coefficient is not *a priori* determined, but it is a consequence of the dynamics, which now involves the magnetic field. In the context of magnetic confinement of hot plasmas, Taylor [32] suggested that the development of self-consistent fluctuations could result in values of the Langevin drag coefficient whose role would be to maximize the diffusion coefficient, thus leading to an "anomalous transport" with a diffusion coefficient that decreases as B^{-1}, instead of the more favorable B^{-2} dependence expected from Eq. (21). Within the Langevin model, this maximal transport is obtained when (in scaled variables) $\Gamma = w$. To gain some insight on this issue from the chaotic perspective, it is informative to exploit the relation shown in Eq. (25). By applying an external electric field, as illustrated in Fig. 9, the values of μ_{Ps}, and μ_{Hs} are independently determined over a range of w. Then using Eq. (25) as an indicator, an effective Langevin Γ can be extracted. The result of such a procedure is shown in Fig. 10 over the range $0.05 \leqslant w \leqslant 5.5$ for a fixed value of the scaled electric field $qEt_0/m\bar{v} = 0.1$. It is seen that the effective value of Γ does not exceed 1.6, a result likely determined by the regulating influence of the internal thermostat of the MKT model, and represented by Eq. (13). This implies that as the magnetic field strength is increased, the condition $\Gamma = w$ is not satisfied. Within the Langevin picture that would suggest that the transport should not be "very anomalous." But as is shown later in Fig. 11, the chaotic diffusion coefficient is significantly larger than expected. Another feature seen in Fig. 10 is that as w increases, the value of Γ fluctuates. It is surmised that these fluctuations are related to possible dynamical resonances between the cyclotron frequency and the intrinsic oscillations of the unmagnetized chaotic motion

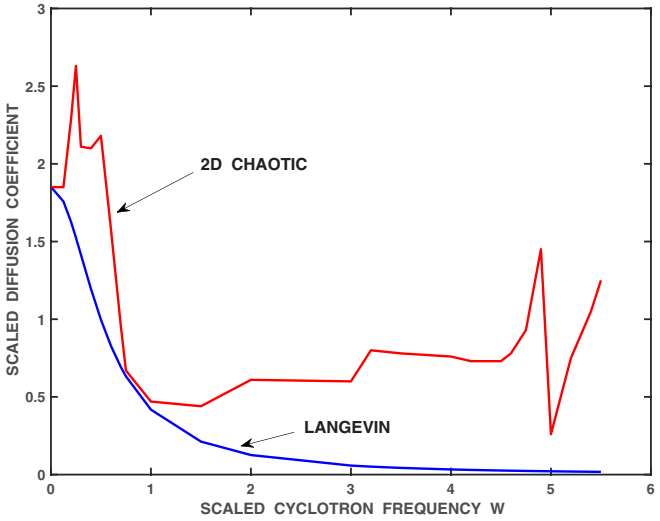

FIG. 11. Magnetic field dependence of the scaled diffusion coefficient over the range $0 \leqslant w \leqslant 5.5$. Red curve, labeled "2D Chaotic," is the result of the 2D chaotic model. Blue curve, labeled "Langevin," is obtained from Eq. (20) with a constant value $\Gamma = 0.5$ that is consistent with the result of the 2D chaotic model for $w = 0$. The sharp peaks and steps in the red curve have been ascertained by making small changes in w to resolve them; they are an intrinsic feature of the chaotic dynamics.

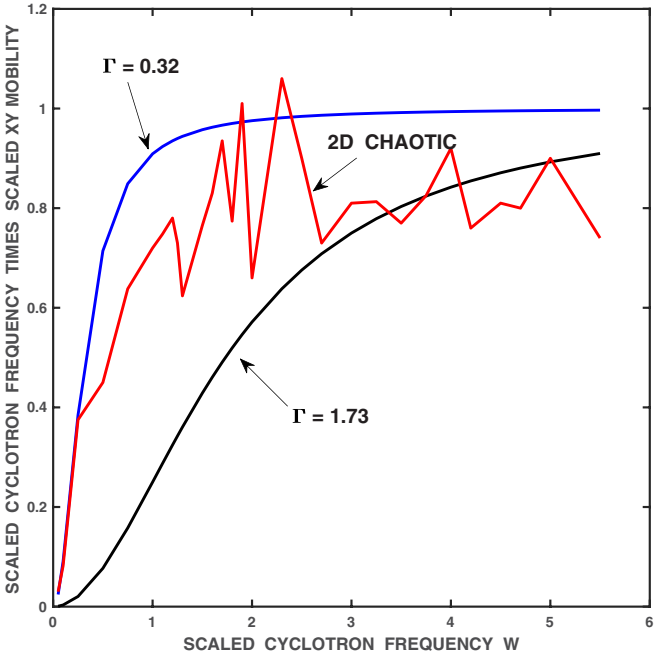

FIG. 12. Magnetic field dependence of the scaled Hall mobility, i.e., the xy component of the (electrical) mobility tensor. To better establish a comparison with the Langevin model the quantity that is displayed is $w\mu_{Hs}$. The red curve, labeled "2D chaotic" is this quantity, calculated from the chaotic thermostat model for a scaled electric field $qEt_0/m\bar{v} = 0.1$ that points along the x direction, and over a range $0.05 \leqslant w \leqslant 5.5$. The blue curve, labeled "$\Gamma = 0.32$," is the prediction of Eq. (23) for this value, and the black curve, labeled "$\Gamma = 1.73$," is a similar prediction for this larger value of the scaled drag coefficient.

represented by the sequence of peaks labeled A–G in Fig. 9. There is also an unexpected behavior in Fig. 10, namely, that the effective value of Γ is negative over a small range of magnetic field values centered around $w = 1.5$; within the Langevin model that is not possible. As is shown in Fig. 13, this negative region is associated with "absolute negative mobility" (ANM) [22–27].

The magnetic field dependence of the scaled diffusion coefficient associated with the 2D chaotic model is represented in Fig. 11 by the red curve, labeled "2D chaotic," over the range $0 \leqslant w \leqslant 5.5$. The comparison blue curve, labeled "Langevin," is obtained from Eq. (20) with a constant value $\Gamma = 0.5$ that is consistent with the result of the 2D chaotic model for $w = 0$. It is seen that the magnetized, 2D chaotic diffusion coefficient is significantly larger than expected from the Langevin model, so in this sense it corresponds to "anomalous transport," but it is not realized by the maximal mechanism suggested by Taylor. It arises from the complex interplay of the self-consistent chaotic fluctuations with the cyclotron motion as suggested by the damping of the peaks A–G in Fig. 9, and the concomitant broadening of the cyclotron resonance. It is also seen from Fig. 11 that the dependence of the diffusion coefficient on magnetic field strength is nonmonotonic; it exhibits localized peaks and steps. These variations are not an artifact of coarse sampling, as they have been ascertained by making small changes in w to resolve them. It is surmised that these structures are a manifestation of the underlying chaotic dynamics, which, upon ensemble average, result in diffusive behavior.

Figure 12 illustrates the magnetic field dependence of the scaled Hall mobility, i.e., the xy component of the (electrical) mobility tensor. To better establish a comparison with the Langevin model the quantity that is displayed is $w\mu_{Hs}$, which according to the Langevin model should asymptote to the value 1 for $w \gg \Gamma$. The red curve, labeled "2D chaotic," is this quantity, calculated from the chaotic thermostat model for a scaled electric field $qEt_0/m\bar{v} = 0.1$ that points along the x direction, and over a range $0.05 \leqslant w \leqslant 5.5$. The blue curve, labeled "$\Gamma = 0.32$," is the prediction from Eq. (23) for this value, and the black curve, labeled "$\Gamma = 1.73$," is a similar prediction for this larger value of the scaled drag coefficient. It is seen that the chaotic result lies between these two predictions, which suggests that the effective drag coefficient increases with increasing magnetic field. The chaotic Hall mobility asymptotes to a mean value $w\mu_{Hs} \approx 0.8$, which is lower than the prediction of the Langevin model. But, significantly, the chaotic mobility shows erratic fluctuations around this mean value that manifest the underlying chaotic nature of the dynamics. These results have been reproduced for arbitrary orientations of the external electric field and by reversing the direction of the magnetic field.

The complementary behavior of the scaled Pedersen mobility, i.e., the xx component of the (electrical) mobility tensor, is shown in Fig. 13. It is obtained simultaneously with the results shown in Fig. 12; i.e., a scaled electric field $qEt_0/m\bar{v} = 0.1$ is applied along the x direction, and the ensemble average velocity along the x direction is calculated over a range of scaled cyclotron frequencies $0.05 \leqslant w \leqslant 5.5$. The results of

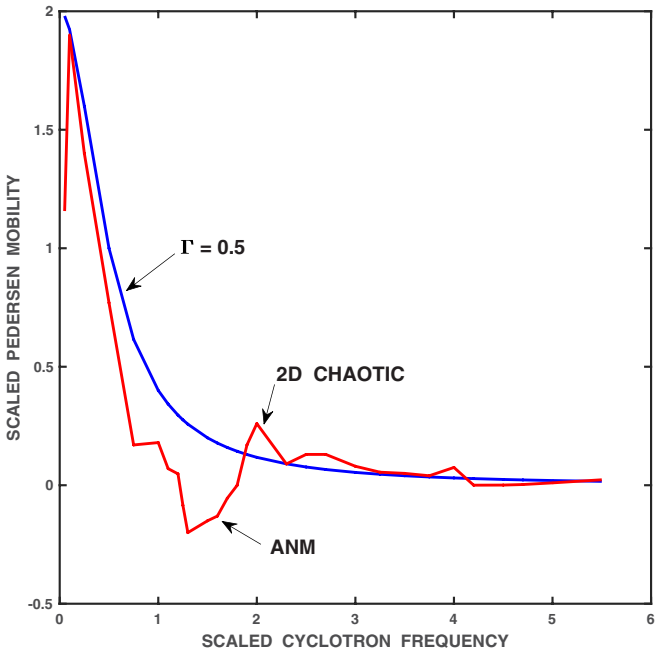

FIG. 13. Magnetic field dependence of the scaled Pedersen mobility, i.e., the xx component of the (electrical) mobility tensor. The red curve, labeled "2D chaotic," is obtained simultaneously with the results shown in Fig. 12; i.e., a scaled electric field $qEt_0/m\bar{v} = 0.1$ is applied along the x direction, and the ensemble average velocity along the x direction is calculated over a range of scaled cyclotron frequencies $0.05 \leqslant w \leqslant 5.5$. The blue curve, labeled "$\Gamma = 0.5$," is the prediction of the Langevin model for this value of the scaled drag coefficient which corresponds to the effective drag coefficient associated with the unmagnetized, chaotic mobility. The arrow labeled ANM identifies a limited range of magnetic field values, centered around $w = 1.5$, in which the chaotic dynamics results in "absolute negative mobility."

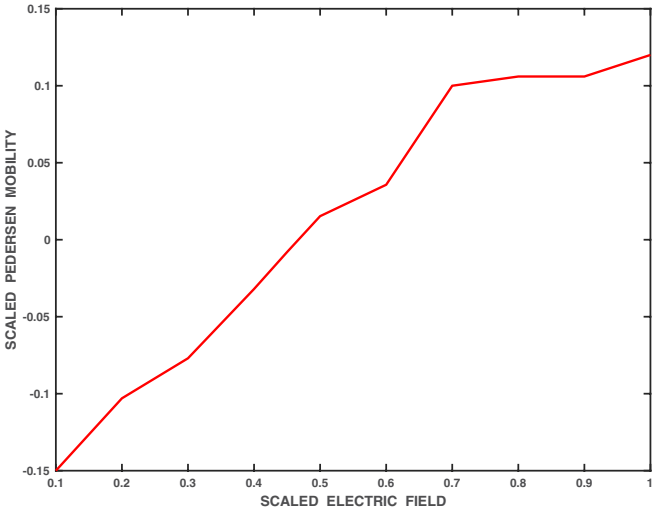

FIG. 14. Threshold behavior of absolute negative mobility (ANM) seen in Fig. 13. Red curve displays the dependence of the scaled Pedersen mobility on the strength of the scaled electric field over a range $0.1 \leqslant qEt_0/m\bar{v} \leqslant 1$, for a scaled cyclotron frequency $w = 1.5$ corresponding to the center of the region of ANM behavior. The phenomenon requires weak electric fields such that $qEt_0/m\bar{v} < 0.5$. Identical (but asymmetrical) results are obtained when the direction of the electric field is reversed.

this procedure are represented by the red curve, labeled "2D chaotic." The blue curve, labeled "$\Gamma = 0.5$," is the prediction of Eq. (22) for this value of the scaled drag coefficient. The choice of this value is based on the result stated in Sec. III, following Eq. (19). It is the effective drag coefficient associated with the unmagnetized, chaotic mobility. On first observation, it appears that the chaotic mobility follows closely the Langevin prediction except for the erratic variations previously seen in the diffusion coefficient and in the Hall mobility. But on closer look, as indicated by the arrow labeled "ANM," one of these fluctuations corresponds to a finite interval in magnetic field strength over which the chaotic system displays "absolute negative mobility." This counterintuitive behavior has received considerable attention in a variety of systems [22–27] in which often the symmetry-breaking process results from scattering by a barrier or ratchet. The surprise here is that ANM arises in the magnetized chaotic thermostat intrinsically from the competition between the fluctuations and the external push, without boundary effects.

As is common in systems in which ANM occurs, the behavior shown in Fig. 13 has a threshold, as is illustrated in Fig. 14. The red curve displays the dependence of the scaled Pedersen mobility on the strength of the scaled electric field over a range $0.1 \leqslant qEt_0/m\bar{v} \leqslant 1$, for a scaled cyclotron frequency $w = 1.5$ corresponding to the center of the region of ANM behavior. It is seen that ANM arises for weak electric fields such that $qEt_0/m\bar{v} < 0.5$. For larger fields, the normal positive mobility returns. Identical (but asymmetrical) results are obtained when the direction of the electric field is reversed.

V. CONCLUSIONS

The present study has demonstrated that the concept of a "chaotic thermostat," consisting of the merger of self-consistent, chaotic fluctuations with a deterministic thermostat, can be extended to motion in two dimensions. The constraint imposed by the azimuthal symmetry of the zero-order system requires that the underlying thermostat must have two internal degrees of freedom, thus the MKT deterministic thermostat is necessary for a suitable formulation. It has been found that the proposed chaotic thermostat results in azimuthally symmetric, Maxwellian velocity distributions with the prescribed temperature, in both unmagnetized and magnetized cases. However, the velocity fluctuations exhibit an exponential frequency spectrum characteristic of chaotic systems and associated with temporal pulses having a Lorentzian shape.

The 2D walks generated by the chaotic thermostat consist of a mixture of long flights and periods of relative localization. The length and direction of the flights, and how long the localization lasts, have the appearance of random events, but the underlying process is based on deterministic rules. The ensuing "chaotic thermal motion" is neither a sequence of Lévy flights nor the Brownian motion associated with the Langevin model. But the ensemble average spatial dispersal

is strictly diffusive, in both the unmagnetized and magnetized cases. This finding provides an additional example of systems [40–42] that exhibit diffusive behavior without explicit stochastic dynamics. For the unmagnetized case the Einstein ratio of diffusion to mobility is essentially 1, within numerical uncertainty, and the "effective collision time" associated with the unmagnetized mobility coefficient is approximately four times the width of the Lorentzian pulses.

The chaotic thermostat has been used to gain insight into the behavior of a thermalized charge in the presence of a weak magnetic field such that the coupling to the heat bath and the magnetic force are comparable, but each has an opposite statistical tendency. The magnetic field tries to generate a delta function velocity distribution and the heat bath a Maxwellian. It is found that the self-consistent chaotic fluctuations allow the attainment of a Maxwellian velocity distribution, but the consequence is that the magnetized transport coefficients exhibit "anomalous behavior," i.e., they depart from the predictions of the Langevin model in which the drag coefficient is constant and the fluctuations are uncorrelated. The most significant departure is in the spatial diffusion coefficient, illustrated by Fig. 11. The chaotic nature of the system manifests in the form of erratic variations in the magnitude of the diffusion coefficient as the strength of the magnetic field is changed. Such a behavior is quite different from the monotonic dependence predicted by the Langevin model, even under the maximal drag condition postulated by Taylor [32]. But similar phenomena has been found for the diffusion coefficient associated with discrete chaotic maps [13,42,43]. The dependence of the Hall mobility on the strength of the magnetic field, illustrated by Fig. 12, is bracketed by predictions of the Langevin model having two different values of the effective drag coefficient. But it also exhibits erratic variations as the magnetic field is increased. The corresponding behavior of the Pedersen mobility follows more closely the Langevin model, illustrated in Fig. 13, but it shows the unexpected appearance of "absolute negative mobility" (ANM) over a limited range of magnetic field strengths. This phenomenon has a threshold; as the strength of the applied electric field is increased the state of positive mobility returns.

In summary, the proposed extension of the chaotic thermostat concept to two dimensions provides a tool for the exploration of more realistic situations in which a competition between thermalization and nonequilibrium conditions exists. It also contributes a deterministic perspective that complements predictions based on the stochastic Langevin model.

ACKNOWLEDGMENTS

This work was performed under the auspices of the Basic Plasma Science Facility (BaPSF) at the University of California, Los Angeles (UCLA), which is jointly supported by the Department of Energy (Grant No. DE-FC02-07ER54918) and the National Science Foundation (Grant No. PHY 1036140). The author thanks M. Poulos for valuable help in the preparation of the manuscript.

[1] G. J. Morales, Phys. Rev. E **97**, 032203 (2018).
[2] S. Nosé, J. Chem. Phys. **81**, 511 (1984).
[3] Wm. G. Hoover, *Computational Statistical Mechanics* (Elsevier, Amsterdam, 1991).
[4] D. J. Evans and G. P. Morris, *Statistical Mechanics of Nonequilibrium Liquids* (Academic Press, New York, 1990).
[5] G. P. Morris and C. P. Dettman, Chaos **8**, 321 (1998).
[6] W. G. Hoover, Phys. Rev. A **31**, 1695 (1985).
[7] G. J. Martyna, M. L. Klein, and M. Tuckerman, J. Chem. Phys. **97**, 2635 (1992).
[8] T. Geisel, A. Zacherl, and G. Radons, Z. Phys. B **71**, 117 (1988).
[9] C. F. Barenghi, C. J. Mellor, J. Meredith, C. M. Muirhead, P. K. H. Sommerfeld, and W. F. Vinen, Philos. Trans. R. Soc. London A **334**, 139 (1991).
[10] T. H. Solomon, E. R. Weeks, and H. L. Swinney, Phys. Rev. Lett. **71**, 3975 (1993).
[11] K. Rateitschak, R. Klages, and Wm. G. Hoover, J. Stat. Phys. **101**, 61 (2000).
[12] I. Golding and E. C. Cox, Phys. Rev. Lett. **96**, 098102 (2006).
[13] G. Forte, F. Cecconi, and A. Vulpiani, Eur. Phys. J. B **87**, 102 (2014).
[14] S. A. Prasad and G. J. Morales, Phys. Fluids **30**, 3475 (1987).
[15] D. Roy and N. Kumar, Phys. Rev. E **78**, 052102 (2008).
[16] P. Tierno, P. Reimann, T. H. Johansen, and F. Sagués, Phys. Rev. Lett. **105**, 230602 (2010).
[17] J. I. Jiménez-Aquino and M. Romero-Bastida, Phys. Rev. E **86**, 031110 (2012).
[18] N. Ohtomo, K. Tokiwano, Y. Tanaka, A. Sumi, S. Terachi, and H. Konno, J. Phys. Soc. Jpn. **64**, 1104 (1995).
[19] D. C. Pace, M. Shi, J. E. Maggs, G. J. Morales, and T. A. Carter, Phys. Plasmas **15**, 122304 (2008).
[20] J. E. Maggs and G. J. Morales, Plasma Phys. Control. Fusion **55**, 085015 (2013).
[21] J. E. Maggs and G. J. Morales, Phys. Rev. E **86**, 015401(R) (2012).
[22] J. L. Mateos, Phys. Rev. Lett. **84**, 258 (2000).
[23] R. Eichhorn, P. Reimann, and P. Hänggi, Phys. Rev. Lett. **88**, 190601 (2002).
[24] A. Ros, R. Eichorn, J. Regtmeier, T. T. Duong, P. Reimann, and D. Anselmetti, Nature (London) **436**, 928 (2005).
[25] L. Machura, M. Kostur, P. Talkner, J. Luczka, and P. Hänggi, Phys. Rev. Lett. **98**, 040601 (2007).
[26] A. Sarracino, F. Cecconi, A. Puglisi, and A. Vulpiani, Phys. Rev. Lett. **117**, 174501 (2016).
[27] R. Chen, L. Nie, C. Chen, and C. Wang, J. Stat. Mech. (2017) 013201.
[28] M. F. Shlesinger, G. M. Zaslavsky, and U. Frisch, editors (eds.), *Lévy Flights and Related Topics in Physics* (Springer, Paris, 1994).
[29] V. Zaburdaev, S. Denisov, and J. Klafter, Rev. Mod. Phys. **87**, 483 (2015).
[30] J. Klafter and G. Zumofen, Phys. Rev. E **49**, 4873 (1994).
[31] P. L. Bhatnagar, E. P. Gross, and M. Krook, Phys. Rev. **94**, 511 (1954).
[32] J. B. Taylor, Phys. Rev. Lett. **6**, 262 (1961).

[33] B. Kursunoglu, Phys. Rev. **132**, 21 (1963).
[34] H. Furuse, J. Phys. Soc. Jpn. **28**, 559 (1970).
[35] Karmeshu, Phys. Fluids **17**, 1828 (1974).
[36] N. Kumar, Phys. Rev. E **85**, 011114 (2012).
[37] V. Lisy and J. Tothova, Transport Theory Stat. Phys. **42**, 365 (2013).
[38] A. Baura, S. Ray, M. Kumar Sen, and B. Chandra Bag, J. Appl. Phys. **113**, 124905 (2013).
[39] H. M. Chun, X. Durang, and J. D. Noh, Phys. Rev. E **97**, 032117 (2018).
[40] T. Geisel and J. Nierwetberg, Phys. Rev. Lett. **48**, 7 (1982).
[41] F. Cecconi, M. Censini, and A. Vulpiani, J. Stat. Mech.: Theory Exp. (2007) P12001.
[42] I. Dana, N. W. Murray, and I. C. Percival, Phys. Rev. Lett. **62**, 233 (1989).
[43] R. Klages and J. R. Dorfman, Phys. Rev. Lett. **74**, 387 (1995).